Fivefold surface of quasicrystalline AlPdMn: Structure determination using low-energy-electron diffraction

M. Gierer* and M. A. Van Hove
Lawrence Berkeley National Laboratory, University of California, Berkeley, California 94720

A. I. Goldman
Department of Physics and Astronomy and the Ames Laboratory, Iowa State University, Ames, Iowa 50011

Z. Shen, S.-L. Chang, P. J. Pinhero, C. J. Jenks, J. W. Anderegg,
C.-M. Zhang, and P. A. Thiel
Department of Chemistry and the Ames Laboratory, Iowa State University, Ames, Iowa 50011
(Received 6 August 1997)

The atomic structure of the fivefold symmetric quasicrystal surface of icosahedral AlPdMn has been investigated by means of a dynamical low-energy-electron diffraction (LEED) analysis. Approximations were developed to make the structure of an aperiodic, quasicrystalline surface region accessible to LEED theory. A mix of several closely similar, relaxed, bulklike lattice terminations is favored, all of which have a dense Al-rich layer on top followed by a layer with a composition of about 50% Al and 50% Pd. The interlayer spacing between these two topmost layers is contracted from the bulk value by 0.1 Å, to a final value of 0.38 Å, and the lateral density of the two topmost layers taken together is similar to that of an Al(111) surface. The LEED structural result is qualitatively consistent with data from ion scattering spectroscopy, which supports an Al-rich termination. [S0163-1829(98)03713-8]

I. INTRODUCTION

Over the past few years, a great deal of attention has been focused on the properties of quasicrystalline surfaces.[1–21] This is partly due to the relatively recent availability of single grains of sufficient size for surface studies.[22–28] Much of the heightened interest, however, is due to reports of unusual surface properties such as oxidation resistance,[29,30] low surface friction,[31,32] superior wear resistance, and other tribological characteristics.[31] Because of these properties, quasicrystalline alloys may find important technological applications, including surface coatings for wear resistance in corrosive environments.

It is not yet entirely clear whether the aperiodic ordering of quasicrystalline alloys[33–35] is responsible, in whole or in part, for the surface properties mentioned above. Nevertheless, the quasicrystals present us with a new opportunity to study the surface structure, topology, and chemistry of fundamentally incommensurate solids in comparison with their periodic cousins. Already, some investigations have shed light on fundamental aspects of quasicrystal surfaces as well as introduced new puzzles. Scanning tunnel microscope (STM) investigations of the decagonal Al-Cu-Co by Kortan *et al.*,[2] and the icosahedral phase of Al-Pd-Mn by Schaub *et al.*,[5,6] prepared by sputtering-annealing cycles in vacuum, have revealed the existence of aperiodic quasicrystalline order at the surface of these alloys, and of atomic-scale features with local fivefold symmetry. After annealing of a AlPdMn surface, fivefold symmetric facets were observed by low-energy-electron diffraction (LEED) and STM, and the surface topology of these facets can be described by a set of atomically flat terraces with steps of two different heights in a succession corresponding to a Fibonacci sequence. STM measurements on cleaved surfaces of Al-Pd-Mn by Ebert *et al.*,[11] however, revealed a rough surface with clusterlike features, thus raising questions as to the effect of surface preparation upon the resulting surface structure. More recently, the twofold surface of Al-Pd-Mn, prepared by sputtering annealing, was subjected to low-energy-electron diffraction measurements. The LEED pattern of this surface indicates its surface is similar to that in the bulk, since the spot positions are what would be expected for the unreconstructed surface.[13]

In this context, it becomes appealing to exploit techniques sensitive to the surface geometry to extract information about the atomic-scale structure of quasicrystalline surfaces. The most well-established of these is dynamical scattering analysis of LEED intensity-voltage (IV) data. For periodic surfaces, this approach has been used successfully to solve the majority of all known detailed surface structures.[36] However, a difficulty arises in applying this technique to quasicrystalline surfaces: because of the aperiodicity, it is not possible to define a unit cell with finite size, and exact fully dynamical calculations of LEED IV curves are therefore not feasible. In this paper, we discuss approximations that help to overcome this difficulty, then apply them to a quantitative LEED analysis of the fivefold symmetric surface of icosahedral AlPdMn. We have already reported preliminary results from this work elsewhere.[12]

While LEED is a well-established method to determine the surface geometry, it is known that LEED IV data are not very sensitive to moderate changes in metal alloy composition.[37] Therefore, we complemented our structure investigation with a technique uniquely sensitive to the chemical composition of the topmost layer, namely, low-energy ion scattering (LEIS).

This paper is organized as follows: First, experimental details are presented in Sec. II. In Sec. III, the approximations used for the calculation of the LEED IV curves of a quasicrystal are derived and discussed, and in Sec. IV, we

present the results of a LEED structural analysis of a specific quasicrystal surface, namely, the fivefold symmetric surface of the icosahedral AlPdMn phase. In Sec. V, relevant results on surface composition from ion scattering spectroscopy are given, followed by a discussion of all the results in Sec. VI.

II. EXPERIMENTAL DETAILS

LEED experiments were performed in an ultrahigh vacuum chamber equipped also for Auger electron spectroscopy, mass spectrometry, ion bombardment, sample heating, sample cooling, and introduction of select gases. Other papers give details about our equipment,[8] methods of sample preparation,[38] and data acquisition and reduction in LEED.[8,39] Our sample is a flat pentagonal wafer, approximately 5×3 mm^2 in surface area, and 1.5 mm thick.

The bulk composition of our sample is $Al_{70}Pd_{21}Mn_9$.[38] In this paper, we exploit the bulk structure analysis of de Boissieu *et al.*, and also compare our results with the STM work of Schaub *et al.* Both of these other groups used samples with slightly different (nominal) bulk composition: $Al_{68}Pd_{23}Mn_9$. The difference between our composition and theirs is probably negligible for our purposes, given that both compositions are well within the limits of stability of the icosahedral phase.

A typical LEED pattern from our sample is reproduced in Fig. 1(a) and a schematic that shows the indexing scheme in Fig. 1(b). Like previous authors, we find that the symmetry and spacing of the LEED beams are consistent with the hypothesis that the fivefold surface of this alloy retains the bulk quasicrystallinity.[8] For the IV analysis, it is important to note that three rings of bright diffraction spots are visible in the energy range 70–280 eV. Each ring consists of 10 spots equidistant from the origin. Each ring of 10 contains two inequivalent sets of 5 spots arranged at the corners of two pentagons. Hence, the IV characteristics can (in principle) be measured for 30 beams—although some are always blocked by the sample manipulator in our front-view geometry. Each set of (up to) 5 symmetry-equivalent spots is averaged, thus reducing the database to 6 symmetry-inequivalent IV curves. The cumulative energy range encompassed by these data is 800 eV. All IV data were measured with the sample at 100 K to minimize Debye-Waller attenuation. We index one of the sets of the innermost ring visible in this energy range as (10 000) and equivalent, although two smaller sets are visible at lower energies, down to 15 eV.

For purposes of structure analysis, the LEED IV curves are acquired at normal incidence. The quality of normal incidence can be judged from Fig. 2, which shows the data for four individual spots, all of which are symmetry equivalent to the (10 000). At perfect normal incidence, these curves should be identical. While this criterion is not met exactly, the shapes, positions, and relative intensities of major features are reasonably reproduced.

Different methods of surface preparation can yield somewhat different surface compositions in this alloy.[38] Therefore, we tested the effect of surface preparation on the IV curves. The result of 5 different treatments on the (symmetry averaged) (10 000) beam is shown in Fig. 3. In all cases, except Fig. 3(f) the sample was initially prepared by 1 keV Ar^+ bombardment for 40 min at 2 to 4×10^{-5} A cm^{-2} (this

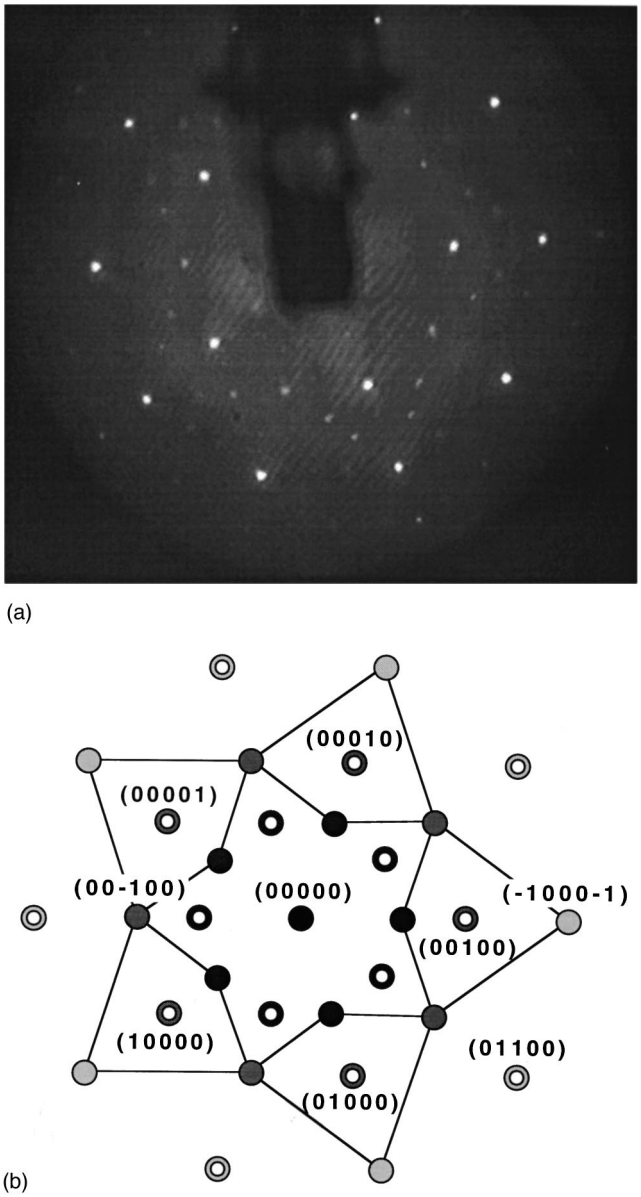

FIG. 1. (a) LEED pattern at 80 eV incident electron energy and normal incidence. The dark shadow at top and middle is the sample manipulator, which obscures some spots. (b) Schematic of the LEED pattern, illustrating the indexing scheme of spots visible in the 70–240 eV range. One set of spots that are symmetry equivalent at normal incidence consists of (10 000); (01 000), (00 100), (00 010), and (00001), 72° apart. Another is the same with negative labels: $(-10\,000)$, $(0-1000)$, etc.

is the current to ground without bias) and at room temperature, followed by various annealing programs. The data used in the structure analysis [Fig. 3(a)] were obtained after annealing at 1000 K for 4 h. Other treatments consisted of annealing at 870 K for 4 h [Fig. 3(b)]; annealing at 870 K for 2 h, then 1050 K for 5 min [Fig. 3(c)]; annealing at 1050 K for 10 min, then 870 K for 2.5 h [Fig. 3(d)]; and annealing at 1100 K for 10 min, then 870 K for 3 h [Fig. 3(e)]. The data for Fig. 3(f) were taken on a different sample. In this case, the treatment was 1 keV Ar^+ bombardment for 15 min at 7.5×10^{-5} A cm^{-2} at room temperature and annealing at 750 K for 30 min. In all cases, a sharp fivefold diffraction pattern

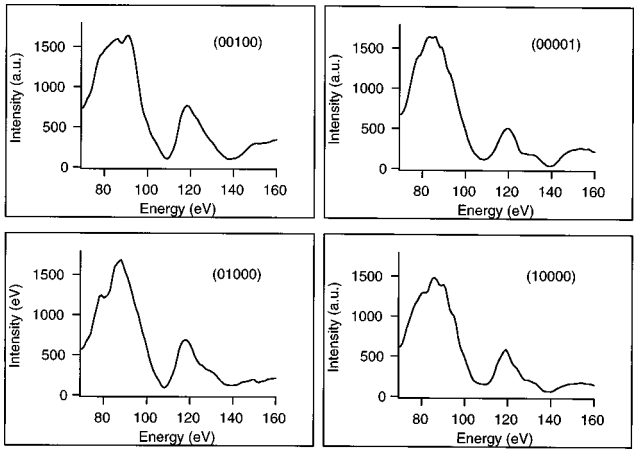

FIG. 2. IV curves of four symmetry-equivalent diffraction spots at normal incidence.

was obtained, and the IV curves were very similar, with one exception: the energy range below 180 eV for the (10-101) spot. In general, however, the data used for the structure analysis are very robust and quite insensitive to details of sample preparation.

It should also be noted that the LEED IV curves are insensitive to possible surface contamination by oxygen, e.g., from background adsorption. Elsewhere, we have shown that deliberate exposure to oxygen serves only to reduce the intensity of the fivefold LEED pattern and increase the background level; the characteristic IV curves do not change in shape.[8] We attribute this invariance to the formation of very small crystalline, or amorphous, regions of aluminum oxide that replace the quasicrystalline regions and contribute to the background intensity, but that do not perturb the long-range structure of the remaining icosahedral matrix.

Low-energy ion scattering was also performed, in a separate chamber and with a separate sample, to gain information about surface composition. X-ray photoelectron spectra (XPS) were acquired simultaneously. Both experiments were performed in a Perkin Elmer Multitechnique Chamber, Model 5500. The base pressure of the chamber was 3×10^{-10} Torr or better. Other details of the XPS measurements are given elsewhere.[9,10] For LEIS, 750 eV $^3He^+$ ions were used with a beam current of 14 nA in a spot with dimensions of approximately 200–800 μm, rastered over a total area of approximately 2 mm$\times$2 mm. With respect to the surface plane, the incident beam impinges on the surface at an angle of 50° and the analyzer collects at an angle of 45°. The angle between the incident beam and the analyzer, projected onto the surface plane, is 69°.

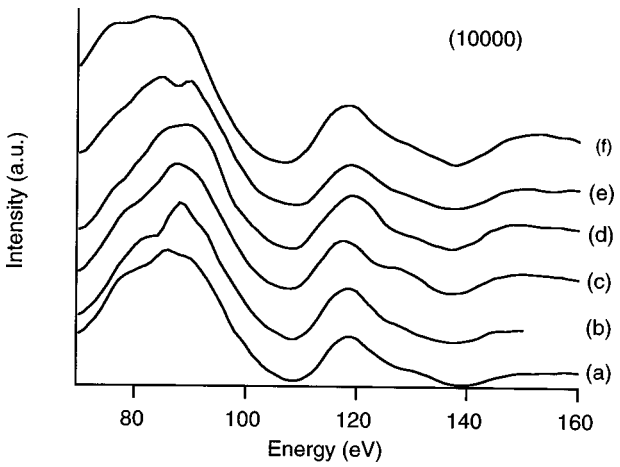

FIG. 3. IV curves of a single diffraction spot, averaged over all symmetry equivalent beams, after various annealing preparations as described in the text.

The sample was cleaned by Ar^+ etching at 4 keV, followed by annealing at 870 K for 15–20 min. The LEIS data were acquired at room temperature. The LEIS experiment was repeated on three separate fivefold samples (each different than the one used in LEED experiments, but prepared similarly).

Sputtering did not occur significantly during the LEIS experiments, based upon the invariance of XPS data acquired before and after the LEIS experiments. It is known that sputtering with Ar^+ changes the surface composition[6,15,38] and the line shape of Mn $2p_{3/2}$ photoelectrons.[10] Neither such change was observed as a result of the LEIS measurement. The composition of the surface and near-surface region, measured with XPS and using sensitivity factors in the PHI Access software, version 5.3c, was $Al_{70}Pd_{22}Mn_8$.

III. DEVELOPMENT OF THEORY

Due to the aperiodicity of a quasicrystal, one has to deal with an infinitely large number of atoms with different scattering properties. In principle, each atom in a quasicrystal has a different chemical environment beyond nearest neighbors, and the scattering properties of an atom depend also on the positions of its surrounding atoms in the case of multiple scattering. In a regular periodic crystal, the number of atoms with different scattering properties is restricted by the size of the two-dimensional surface unit cell and the number of atomic planes to be taken into account, which is determined by the inelastic mean-free path of the electrons. For a quasicrystal, however, this consideration does not hold since it is not possible to define a surface unit cell of finite size. Since the LEED calculation time increases strongly with the number of atoms with different scattering properties, exact calculations of the LEED IV curves are impossible. In order to reduce the number of atoms with different scattering properties used in the calculation, we have to apply efficient approximations that we describe in the following.

As a starting point for the LEED analysis, we used the bulk structure of $Al_{68}Pd_{23}Mn_9$ determined by x-ray and neutron diffraction.[40] This provides atomic hypersurfaces located on the nodes of a six-dimensional bcc lattice. The three-dimensional structure can then be generated as a cut through the six-dimensional lattice. While spherical atomic hypersurfaces were used to model the x-ray data in Ref. 40, we used a slightly modified model, with the outer shells of the atomic hypersurfaces having tricontahedral shapes.[41] This model leads to reasonable bond lengths in the three-dimensional structure while some of the bond lengths are unreasonably short when using spherical hypersurfaces. Otherwise, the geometry and the chemical composition of the atomic planes is very similar, and the distances between the (denser) atomic planes are identical.

It turns out that about 60% of the atoms are in icosahedral

clusters, the pseudo-Mackay icosahedra, thus locally reflecting the overall icosahedral symmetry of the quasicrystal. The densest planes show up perpendicular to the fivefold direction. Two bulk planes perpendicular to a fivefold axis are shown in Fig. 3(a) of Ref. 12, while in Fig. 3(b) of Ref. 12, the planes are drawn at their respective depths z. [Note that in Fig. 3(a), the registries of these two planes are preserved in the two panels, so that the two figures can be superimposed directly.] As a starting point for our LEED analysis, we assumed that each such plane might represent a surface termination. The assumption of a flat surface is justified by the STM measurements of Schaub *et al.* that revealed the occurrence of atomically flat terraces with fivefold symmetry after annealing of a AlPdMn quasicrystalline sample. Note that the surface preparation of Schaub *et al.* was quite similar with ours as described in Sec. II and Ref. 38.

For the LEED analysis, we first analyzed a large set of such terminations lying in an arbitrarily chosen box with a surface area of 100×100 Å^2 and a depth of 50 Å. As a result of quasiperiodicity, all of these terminations are in principle different. Many of them have, however, very similar chemical compositions and geometries so that only a finite number of qualitatively different terminations must be considered. Each of these surfaces is represented as a stack of individual planes (parallel to the surface) of coplanar atoms, each such plane having its own particular composition and density.

In order to reduce the number of atoms with different scattering properties, we divided the crystal into planes of atoms with a particular composition and density and assumed that all atoms of a certain plane have the same scattering properties. In the first step of the structure analysis, the average t-matrix approximation (ATA) (Refs. 37,42,43) was applied to each plane with its own bulklike composition to generate a unique atom with average scattering properties. The scattering matrices t_i of the individual atoms within one plane are replaced by an averaged weighted scattering matrix, depending on the average chemical composition c_i of the plane

$$\langle t\rangle = c_{\mathrm{Al}}t_{\mathrm{Al}} + c_{\mathrm{Pd}}t_{\mathrm{Pd}} + c_{\mathrm{Mn}}t_{\mathrm{Mn}}. \tag{1}$$

This approach is justified by the fact that LEED IV curves, at least for chemically disordered alloys, are in general relatively insensitive to the chemical identity of the individual atoms, compared to their positions. One has to be careful, however, because the AlPdMn quasicrystal has chemical order, which may have a stronger influence on the LEED intensities. Therefore, we performed the final structural refinements without using the ATA.

For the calculation of multiple scattering, the variable local environments of the atoms in a particular plane were replaced by a fixed, simplified average geometry, which will be explained further below. In the following, we refer to this approximation as ''average neighborhood approximation.'' In order to obtain a simplified expression, we considered the scattering amplitude for a large composite layer in the ''giant matrix'' notation (see, e.g., Ref. 44):

$$f(\mathbf{k}_g) = \frac{1}{A}\sum_{L,L'} A_L(\mathbf{k}_g^-)\left\{\sum_{\alpha,i_\alpha} e^{-i\mathbf{k}_g^-\mathbf{r}_{i_\alpha}} \sum_{\beta,j_\beta} [1-X]^{-1}_{Li_\alpha,L'j_\beta} e^{i\mathbf{k}_0^+\mathbf{r}_{j_{\beta\langle t_l 1\rangle\beta}}}\right\} B_{L'}(\mathbf{k}_0^+).$$

Here, $e^{i\mathbf{k}_0^+\mathbf{r}_{j_\beta}}$ corresponds to the propagation of the incident wave $\mathbf{k}_0^+$ to atom j in plane β, the large, ''giant'' matrix $[1-X]^{-1}_{Li_\alpha,L'j_\beta}$ describes all scattering events beginning at atom j in plane β and ending at atom i in plane α in angular momentum space, and $e^{-i\mathbf{k}_g^-\mathbf{r}_{i_\alpha}}$ stands for the outgoing wave coming from atom i in plane α. $A_L(\mathbf{k}_g^-)$ and $B_{L'}(\mathbf{k}_g^+)$ are quantities dependent on spherical harmonics, prefactors, etc.[44] A is the surface area taken into account in the calculation, in our case a circle with a diameter of 100 Å.

Since we assume that all atoms in plane β are coplanar, the phase factor $e^{i\mathbf{k}_0^+\mathbf{r}_{j_\beta}}$ is equal for all atoms in plane β for normal incidence. We assume that all atoms in plane α have the same environment and replace the propagator matrix describing the propagation from the atoms in plane β to atoms in plane α by its average:

$$\sum_{j_\beta}[1-X]^{-1}_{Li_\alpha,L'j_\beta} \approx \frac{1}{I_\alpha}\sum_{j_\alpha}\sum_{j_\beta}[1-X]^{-1}_{Li_\alpha,L'j_\beta} := \langle[1-X]^{-1}\rangle_{L\alpha,L'\beta}$$

for all atoms in plane α.

Thereby, I_α is the number of atoms in plane α and the brackets stand for averaging over all atoms in plane α.

This leads to the following, simplified expression:

$$f(\mathbf{k}_g^-) = \sum_{L,L'} A_L(\mathbf{k}_g^-)\left\{\sum_\alpha S_\alpha(\mathbf{g}) e^{-ik_{gz}^- z_\alpha} \times \sum_\beta \langle[1-X]^{-1}\rangle_{L\alpha,L'\beta} e^{ik_0^+ z_\beta}\langle t_l\rangle_\beta\right\} B_{L'}(\mathbf{k}_0^+), \tag{2}$$

with $S_\alpha(\mathbf{g}) = 1/A\Sigma_{i_\alpha} e^{-i\mathbf{g}\mathbf{r}_{i_\alpha}} =$ lattice factor of plane α.

We still have to find an expression for the X matrix. Therefore, we simplify $\langle[1-X]^{-1}\rangle_{L\alpha,L'\beta}$ by assuming an averaged propagator matrix $\langle G\rangle$:

$$\langle[1-X]^{-1}\rangle_{L\alpha,L'\beta} \approx [1-\langle X\rangle]^{-1}_{L\alpha,L'\beta}$$

with $\langle X\rangle_{L\alpha,L'\beta} = t_{\alpha l}\langle G\rangle_{L\alpha,L'\beta}$

and

$$\langle G\rangle_{L\alpha,L'\beta}=-\frac{1}{I_\alpha}\sum_{i_\alpha=1}^{I_\alpha}\sum_{j_\beta=1}^{I_\beta}4\pi i\,\frac{2m}{\hbar^2}$$

$$\times\sum_{L_1}a(L,L',L_1)i^{l_1}h_{l_1}^{(1)}(k_0|\mathbf{r}_{i_\alpha}-\mathbf{r}_{j_\beta}|)$$

$$\times Y_{l_1m_1}[\Omega(\mathbf{r}_{i_\alpha}-\mathbf{r}_{j_\beta})].$$

In addition, $a(L,L',L_1)$ are Clebsch Gordon coefficients, $h_{l_1}^{(1)}$ and $Y_{l_1m_1}$ are Hankel functions and spherical harmonics, respectively, and I_α,I_β give the number of atoms in the planes α and β, respectively.[44]

In many cases, especially for structures with high symmetry and with normal incidence, the G-matrix elements with $m\neq m'$ are much smaller than the diagonal elements with $m=m'$. This is exploited in the ''diagonal dominance'' approximation.[45] Thus, we consider only G-matrix elements with $m=m'$, i.e., only terms with $m_1=0$. This leads to the following, simpler expression for the propagator matrix:

$$\langle G\rangle_{L\alpha,L'\beta}\approx-\sum_{d_{\alpha\beta}}4\pi i\,\frac{2m}{\hbar^2}N_{d_{\alpha\beta}}\sum_{l_1}a(L,L',l_1)i^{l_1}h_{l_1}^{(1)}$$

$$\times(k_0d_{\alpha\beta})\left(\frac{2l_1+1}{4\pi}\right)P_{l_1}\{\Omega[d_{\alpha\beta}/(z_\alpha-z_\beta)]\}. \tag{3}$$

Here, $d_{\alpha\beta}$ is the distance between an atom in plane α and an atom in plane β, and $N_{d_{\alpha\beta}}$ the average number of neighbors (in plane β) of an atom in plane α at distance $d_{\alpha\beta}$. P_l stands for a Legendre polynomial.

With this approximation, we can perform the calculation with a small number of atoms with different scattering properties. If we take atoms down to 8 Å into account, we obtain about 10 planes, i.e., 10 atoms with different scattering properties; contributions of deeper atoms do not influence the IV curves significantly since they are strongly damped due to inelastic scattering events. These events are similar in strength in quasicrystals compared to other materials, as judged by the measured peak width in LEED IV curves (this peak width is proportional to the imaginary part of the crystal potential, which in turn is simply related to the electron mean-free path). The calculation time is now faster than the time required for a regular crystal with a unit cell containing 10 atoms when using the ''giant matrix method'' (note that the diagonal dominance approximation saves a considerable amount of computing time). Useful, also, is the fact that one need only calculate the scattering properties for the particular incident and exit beam directions of interest.

Since it is not possible to provide an ''exact'' theory for comparison and testing, we use another, qualitatively different approximation for reference, namely, the quasidynamical approximation. The (reasonable) assumption is that the differences between the two approximations will be qualitatively similar to the differences between either approximation and the exact result (the qualitative fit seen in the final comparison of our approximate theory with experiment confirms the validity of this assumption). The checks were performed on the configuration illustrated in Fig. 4. Within the quasidynamical approximation,[46,47] the multiple scattering within single atomic planes or ''composite'' layers is neglected (composite layers consist of more than one atomic plane, as shown by brackets in Fig. 4), while scattering between different planes or layers is taken exactly into account by layer stacking (a method similar to layer doubling, for nonperiodic stacks of layers).[44] With this approach, we must treat layers with a large density and a small interlayer spacing as composite layers because the layer stacking method does not converge otherwise. This represents a net loss of accuracy, since all multiple scattering within a composite layer is neglected.

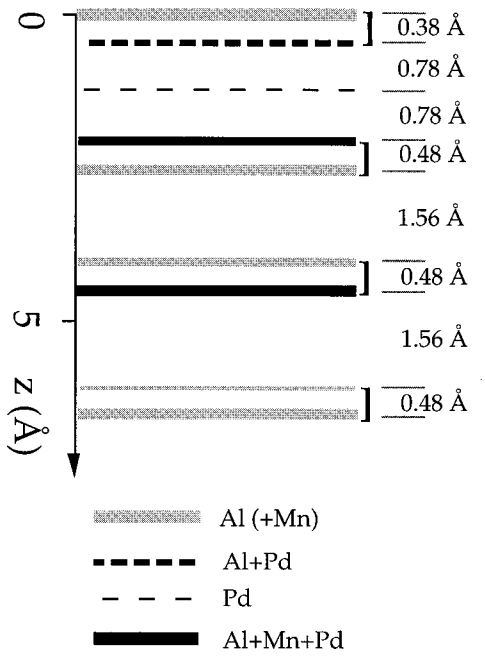

FIG. 4. Configuration of icosahedral AlPdMn used for the test calculations for the ''average neighborhood approximation'' and the quasidynamical approximation; the planes are drawn at their respective depths z as bars with thickness proportional to the atomic density in each plane, together with their approximate composition shown in shades of gray (see labeling below). The planes combined by brackets are treated as composite layers in the quasidynamical approximation.

In the quasidynamical approximation, neglecting intralayer scattering, one obtains the following kinematic expression for the scattering matrix of a composite layer from beam $\mathbf{g}'$ to beam $\mathbf{g}$

$$M_{\mathbf{gg}'}^{\pm\pm}\propto\sum_{\alpha=1}^{n\text{lay}}\langle f_\alpha(\mathbf{k}_{g'}^{\pm}-\mathbf{k}_g^{\pm})\rangle\cdot S_\alpha$$

$$\times(\mathbf{g}-\mathbf{g}')\cdot\exp[i(k_{g'z}^{\pm}-k_{gz}^{\pm})z_\alpha], \tag{4}$$

whereby $n$lay corresponds to the number of planes within the composite layer,

$$\langle f_\alpha(\mathbf{k}_{g'}^{\pm}-\mathbf{k}_g^{\pm})\rangle=\frac{2\pi}{k}\sum_l(2l+1)P_l(\cos\Theta)\langle t_l\rangle_\alpha$$

is the atomic scattering factor in plane a (averaged according to the ATA method), and $S_\alpha(\mathbf{g}-\mathbf{g}')=1/A\Sigma_{i_\alpha}\exp[-i(\mathbf{g}-\mathbf{g}')\mathbf{r}_{i_\alpha}]$ is the lattice factor of the plane a.

The quasidynamical method is, however, rather time consuming compared to the ''average neighborhood'' approach since one has to deal with a large number of beams for which the scattering matrix has to be calculated. (This is because one must provide a good plane-wave expansion of the wave field between planes or layers.) For a quasicrystalline surface, we are theoretically confronted with an infinite number of Bragg reflections which are dense in k space. Almost all of these reflections have, however, systematically very small intensities and are not visible in the LEED pattern. In order to select those beams that we must take into account, we utilized the STM and LEED results of Schaub *et al.* who showed that the quasicrystalline long-range order parallel to the surface can be described by a Fibonacci pentagrid with narrow and wide lattice line separations close to 7.38 Å and 11.94 Å; these values can be deduced also from the bulk model (see Refs. 4 and 5). In a first step, we have calculated the Fourier transform of such a Fibonacci pentagrid. The Fourier transform corresponds to a kinematical, i.e., single-scattering, LEED simulation applied to a simple uniform atom located at each grid intersection in one plane: the resulting beam intensities give an order-of-magnitude idea of the importance of individual beams. We used only beams with an intensity larger then a certain critical value, typically about 1/100 of the intensity of the (00 000) beam. The number of beams can be further reduced if beams are omitted for which the lattice factor is small for all planes of the quasicrystal. We must, however, still include about 100 to 300 beams after this procedure, (depending on the energy that varies between 70 and 280 eV in our experimental data) for which we have to calculate the scattering matrices (4).

Test calculations using the ''average neighborhood approximation'' and the quasidynamical approximation generally lead, for this surface, to similar IV curves. For these calculations, the LEED program by W. Moritz[48] was modified, and the ''average neighborhood'' approach [Eqs. (2) and (3)] and the quasidynamical method [Eq. (4)] were implemented. In Fig. 5, IV curves obtained with the ''average neighborhood'' approach are compared with those calculated quasidynamically. The calculations were performed with 9 atomic planes for the termination shown in Fig. 4. The good agreement between the curves obtained with the different approximations can be quantified using the Pendry R factor,[49] which takes a value of 0.23. This value would be considered rather good for a theory experiment comparison for a complex surface structure.

It is also possible to use the ''average neighborhood approximation'' without the ATA. In this case, each plane is divided into two or three subplanes such that each subplane contains only one chemical species. The calculation time, however, increases because we have to deal with more atoms with different scattering properties, in our case with about 20 atoms instead of 10 atoms with the ATA. Calculations with and without the ATA shown in Fig. 5, using the configuration depicted in Fig. 4 as input, demonstrate that most of the IV curves are again similar.

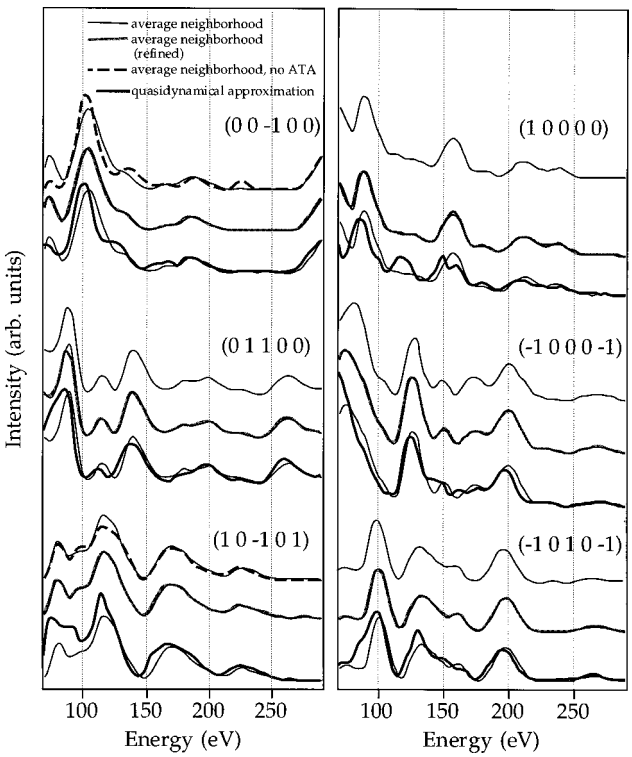

FIG. 5. Comparison of calculated IV curves for different approximations: the ''average neighborhood'' approach (repeated as thin lines for comparison with the other approximations), the same without ATA, the quasidynamical approximation, and the ''refined average neighborhood'' approach; for the local geometries used in the ''refined average neighborhood approach,'' see Table I.

A further refinement of the ''average neighborhood approximation'' approach takes into account that, while the long-range neighborhoods of all atoms are different, the short-range neighborhoods fall into a relatively few classes of identical local neighborhoods. Considering the limited electronic mean-free path, the local neighborhood is far more important in LEED than the distant neighborhood. We thus put only atoms with similar local environment together in one subplane. In so doing, the approximation that the scattering properties of all atoms within a subplane are equal should be more accurate. One can, for example, assume that the local environments of two atoms are similar if the nearest-neighbor distances and the numbers of nearest neighbors (coordination) are equal. In order to refine our approximation, we first determined the nearest-neighbor distance and the coordination for the atoms in the topmost four planes of the termination shown in Fig. 4. We separated all atoms within the first four planes in different layers that do not have the same nearest-neighbor distance or coordination and calculated IV curves using the ''average neighborhood approximation.'' This procedure yielded 12 inequivalent atoms within the topmost four planes to be dealt with. Details about these atoms, including local geometries and concentrations, are given in Table I. As shown in Fig. 5, the calculation leads to IV curves which are almost identical with those performed with only one atom per plane. The close similarity of these curves is another indication that the ''average neighborhood'' approximation is reliable for the fivefold surface of AlPdMn.

TABLE I. Refinement of the ''average neighborhood'' approximation. Atoms with different coordination and nearest-neighbor distance are separated into different layers (details see text). The bulk termination shown in Fig. 4 yields the nearest-neighbor (NN) distance, the number of nearest neighbors (coordination), and concentrations for the first 12 layers given here.

Layer	z (Å)	NN distance	No. of nearest neighbors	Lateral density (atoms/10 000 Å^2)	c_{Al} (%)	c_{Pd} (%)	c_{Mn} (%)
1	0.10	2.57 Å	3	761	98%		2%
2	0.10	2.57 Å	4	41	62%		38%
3	0.10	2.57 Å	5	69	2%		98%
4	0.48	2.57 Å	4	148	90%	10%	
5	0.48	2.57 Å	5	116	86%	14%	
6	0.48	2.57 Å	6	99	30%	70%	
7	0.48	2.57 Å	7	97	0%	100%	
8	1.26	2.81 Å	11	112		100%	
9	2.04	2.57 Å	4	11	100%	0%	0%
10	2.04	2.57 Å	5	44	86%	14%	0%
11	2.04	2.57 Å	6	149	53%	40%	7%
12	2.04	2.57 Å	7	365	8%	71%	21%

To summarize this section, we have with the ''average neighborhood'' approach an approximation at hand which takes many of the most important scattering paths within a quasicrystal properly into account. Within this approach, the scattering properties of all atoms in a plane are assumed to be equal, and the average neighborhood of an average atom in a given plane is described by a kind of radial distribution function: a representative number of neighbor atoms is distributed uniformly on rings, with proper polar angles but without regard to proper azimuthal angles. This local ''cluster'' is summed over in the sense of the lattice sum familiar in the X matrix of LEED theory. The X matrix, which describes the propagation of the electron wave field within layers, is thereby assumed to be independent of the azimuthal angle; this works best at normal incidence, as used in the experiment. Inversion of the X matrix then introduces multiple scattering paths within the layers to infinite order. This is evidenced by checks using the quasidynamical approximation. Within the ''average neighborhood'' approach, we can calculate IV curves of a quasicrystal with a small number of atoms with different scattering properties, typically about 10. The approximation was checked for the $Al_{70}Pd_{21}Mn_9$ system, but it should work also for other quasicrystals, especially if they consist of weaker scatterers, compared to Mn or Pd (as, for example, the icosahedral phases of AlLiCu and AlCuFe). In the following section, we use this approach to analyze the surface structure of icosahedral AlPdMn.

IV. LEED STRUCTURAL RESULTS

In analyzing the experimental LEED data, we first assumed single terminations of the bulk, i.e., no mix of terminations due to possible steps. For the calculations, we used 9 relativistically calculated phase shifts of Al, Pd, and Mn. Temperature effects were described using temperature-dependent phase shifts and a Debye temperature of 480 K for Al, Pd, and Mn. The Pendry R factor was used for comparison between theory and experiments, and error bars were derived from the variance of the R factor.[49] For structural refinement, intensity mixing over different terminations and simultaneous optimization of the perpendicular positions of the topmost planes with respect to the Pendry R factor was performed; therefore, the linear LEED approximation[50] in combination with the Powell optimization scheme was applied. Linear LEED works very well for the AlPdMn system, at least as long as the deviations between trial and reference structure are smaller than about 0.2 Å (which was always the case in our analysis).

To start the structural analysis, the perpendicular positions of the topmost two atomic planes were optimized for each termination within a cube with a surface area of 100×100 Å^2 and a depth of 50 Å, chosen arbitrarily to represent an average piece of bulk quasicrystal. Two inequivalent surface orientations have to be checked, related to each other by a rotation of 180°. One of these orientations gave, however, very bad R factors for all tested terminations and can be ruled out. The other orientation yielded R factors varying from about 0.42 to 0.85 for the different terminations, as shown in Fig. 6. The best terminations have two features in common. First, they consist of a dense pair of outermost atomic planes with an interlayer spacing of about 0.4 Å. Second, the outermost of these two planes is composed primarily of Al, mixed with 0 to 16% Mn, while the innermost of this pair of planes consists mainly of Al and Pd and only small amounts of Mn.

Next, one has to take into account that terraces with different terminations, separated by steps, are present on the surface. In order to model the case of terraces, different terminations were averaged together by intensity mixing with equal weight. After mixing the intensities of the different terminations, we optimized the perpendicular positions of the four topmost planes. By averaging over different terminations one can, however, introduce an arbitrarily large number of parameters in the fit procedure. In order to restrict the number of fit parameters, we assume the layer distances in all terminations taken into account in the mixing to be equal; this is justified because the nonmixed terminations giving the best R factors are quite similar, and the bulk values of the topmost interlayer spacings between the denser atomic planes are identical (see Fig. 6). In this way, we get for a given group of terminations only five fit parameters, namely, the perpendicular positions of the topmost four layers and the real part of the inner potential.

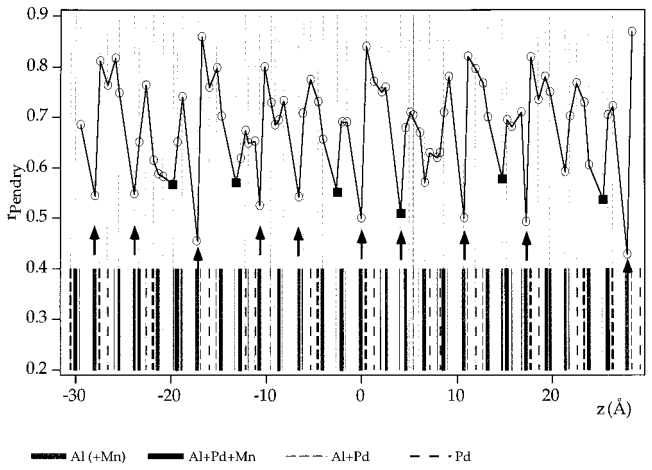

FIG. 6. *R* factors for different terminations of bulk icosahedral AlPdMn, depending on the surface height *z* of the termination. (For each plane shown as a vertical bar, the surface consists of this plane and all planes with higher *z* values; planes with smaller *z* values are cut away). The terminations giving the best *R* factors are marked by arrows [see also Fig. 8(a)]. The configuration marked by squares belong to a group of terminations with a somewhat different geometry [see Fig. 8(b)]; the structure analysis reveals that terminations marked by full arrows probably prevail (see text). In the lower part, the atomic planes are shown, at their respective depths *z*, as bars with thickness proportional to the atomic density in each layer.

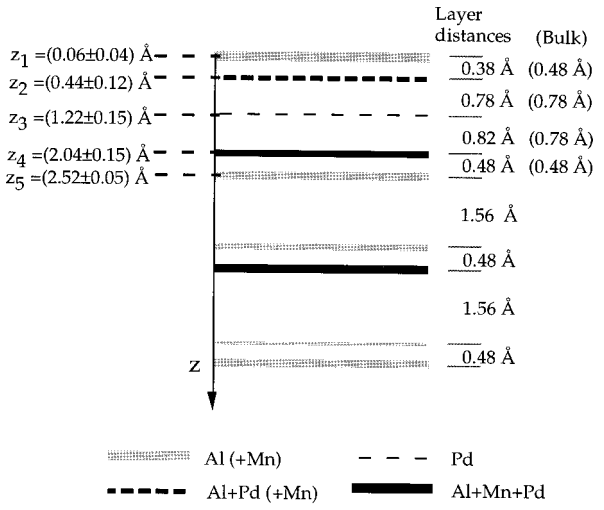

FIG. 7. Optimum geometry found in the LEED structural analysis; the first four interlayer spacings were optimized (corresponding bulk values are shown in parentheses); deeper interlayer spacings were kept fixed at their bulk values. The planes are drawn at their respective depths *z*, as bars with thickness proportional to the atomic density in each plane, together with their approximate composition, as labeled below.

For the mixing, we took the 10 terminations giving the best *R* factors (indicated by the arrows in the *R* factor plot in Fig. 6) and mixed them with equal weight. In this way, the *R* factor could be reduced to 0.31. The optimum geometry is shown in Fig. 7 and Table II. The topmost plane is relaxed inwards by 0.06 ± 0.04 Å while the positions of deeper atomic planes are close to their bulk values. The distance between the topmost and second plane of 0.38 ± 0.13 Å is contracted by about 0.1 Å compared to its bulk value of 0.48 Å. Refinement of the positions of deeper planes does not lead to a significant *R* factor improvement, and neither does an optimization of the weight factors of the terminations. The average chemical composition of the topmost atomic planes, calculated for the bulk like terminations, is 93% Al and 7% Mn for the topmost plane, and 49% Al, 42% Pd, and 9% of Mn for the second plane. The average composition of the two topmost planes taken together is $Al_{77}Pd_{15}Mn_8$. All of these values are compiled also in Table II; the averaged layer densities are given in Fig. 8(a). The averaged lateral density of the two topmost planes taken together is 0.136 atoms/Å^2, a value comparable to that of a single plane of the close-packed Al(111) surface; this indicates a rather densely packed surface. Thereby, the density of the topmost plane is higher than for the second plane for the majority of the terminations. The IV curves calculated for the optimum geometry, obtained after intensity mixing over the terminations marked by arrows in Fig. 6 and optimization of the first four interlayer spacings (see Table II), are compared with the experiment in Fig. 2 of Ref. 12. [Note, however, that one spot was mistakenly labeled as (-1100-1) in Ref. 12; it should have been (-1010-1).]

A closer look at the configurations yielding the better *R* factors reveals that there are terminations that were not taken into account in the mixing and give *R* factors which are only slightly worse. Most of these terminations fall into a group marked by squares in Fig. 6. In Fig. 8(b), the geometry of these terminations is shown. An Al plane on top is followed by a mixed Al-Pd-Mn layer at a distance of 0.48 Å; in contrast to most of the optimum terminations marked by arrows in Fig. 6, the density of the second plane is larger than that of the topmost plane. A look at Fig. 8 reveals differences also in deeper layers. The terminations marked by arrows in Fig. 6 have a dense plane 2.04 Å underneath the surface, which has only small density or is missing for the terminations marked by squares. There are also terminations sharing features of both groups, one of which can be seen in Fig. 6 at $z = 4.08$ Å (thereby, *z* describes the position of the topmost plane, and the *z* axis points towards the bulk).

A mixing of the terminations marked by squares in Fig. 6 with optimization of the topmost interlayer spacings yielded only an *R* factor of 0.45, compared to 0.31 with the configurations marked by arrows. Hence, it can be ruled out that these terminations are solely present at the surface. A mixing of the optimized configurations for the ''square'' and ''arrow'' terminations with equal weight does not change the *R* factor significantly. Refined calculations without the ATA described below, however, lead to a significant worsening of the *R* factor when adding the terminations marked by squares in Fig. 6, so that there is evidence that the surface consists mainly of terminations like those marked by arrows.

In the calculations described above, we neglected the chemical ordering parallel to the surface by applying the average *t* matrix approximation for the scattering factors of the atomic planes. Next, we took this chemical ordering into account, by performing calculations without the ATA. For structural refinement, we averaged over different terminations and optimized the perpendicular positions of the topmost atomic planes. These calculations lead, however, to worse *R* factors than calculations with the ATA (Table II). After averaging over the terminations yielding the best *R*

TABLE II. Optimized Pendry R factor and z positions of the atomic planes after intensity mixing of terminations marked by arrows in Fig. 6 and averaged chemical positions (position of the topmost layer in Fig. 6: $z=-27.96$, -23.88, -17.28, -10.68, -6.60, 0.00, 4.08, 10.68, 17.28, and 27.96 Å). The z axis points towards the bulk, and $z=0.0$ is the position of the topmost layer in the unrelaxed bulk configuration. Shown are the results for calculations with and without ATA, and with various Mn and Al concentrations in the topmost and second layer.

		Optimum geometry	Chemical composition		
	R_P	Vertical positions of layer 1-4	layer 1	layer 2	layer 1+2
ATA, bulklike chemical comp.	0.31	$z_1=(0.06\pm0.04)$ Å	93% Al	49% Al	77% Al
		$z_2=(0.44\pm0.12)$ Å	0% Pd	42% Pd	15% Pd
		$z_3=(1.19\pm0.15)$ Å	7% Mn	9% Mn	8% Mn
		$z_4=(2.04\pm0.15)$ Å			
		$z_5=(2.52\pm0.05)$ Å			
ATA, Mn replaced by Al in 1st layer	0.32	$z_1=(0.06\pm0.04)$ Å	100% Al	49% Al	82% Al
		$z_2=(0.44\pm0.12)$ Å	0% Pd	42% Pd	15% Pd
		$z_3=(1.19\pm0.15)$ Å	0% Mn	9% Mn	3% Mn
		$z_4=(2.04\pm0.15)$ Å			
no ATA, bulklike chemical composition	0.43	$z_1=(0.08\pm0.05)$ Å	93% Al	49% Al	77% Al
		$z_2=(0.45\pm0.10)$ Å	0% Pd	42% Pd	15% Pd
		$z_3=(1.22\pm0.15)$ Å	7% Mn	9% Mn	8% Mn
		$z_1=(2.03\pm0.15)$ Å			
no ATA, Mn replaced by Al in 1st layer	0.37	$z_1=(0.06\pm0.04)$ Å	100% Al	49% Al	82% Al
		$z_2=(0.43\pm0.08)$ Å	0% Pd	42% Pd	15% Pd
		$z_3=(1.19\pm0.15)$ Å	0% Mn	9% Mn	3% Mn
		$z_4=(2.04\pm0.15)$ Å			
no ATA, Mn replaced by Al in 1st and 2nd layer	0.37	$z_1=(0.06\pm0.04)$ Å	100% Al	58% Al	85% Al
		$z_2=(0.43\pm0.08)$ Å	0% Pd	42% Pd	15% Pd
		$z_3=(1.20\pm0.15)$ Å	0% Mn	0% Mn	0% Mn
		$z_4=(2.07\pm0.15)$ Å			

factors (see arrows in Fig. 6), an R factor of 0.43 was obtained (compared to 0.31 with ATA). The positions of the topmost atomic planes are nevertheless almost identical with those obtained with the ATA method, indicating that the optimum structure depends little on the approximation used.

Mixing the terminations marked by squares in Fig. 6 together with the terminations marked by arrows leads to a worsening of the R factor without ATA. To this end, the vertical positions of the topmost atomic planes were optimized, leading to a R factor value of only 0.56 (see Table III). The resulting IV curves were mixed with those obtained for the optimum configuration of the terminations marked by arrows. It turns out that the R factor gets significantly worse if more than 30% of the surface is covered with the terminations marked by squares in Fig. 6.

The worsening of the R factor without the ATA method could have several reasons: either details of the geometry are still not correct, or the chemical composition and ordering within the fivefold symmetric planes is different in the surface region than in the bulk. The experiments with low ion scattering spectroscopy described in Sec. V, for example, revealed that there is only little or even no Mn at the surface.

Therefore, we varied the chemical composition of the topmost plane and replaced Mn by Al. All calculations were done by mixing over the terminations marked by arrows in Fig. 6 and optimization of the four topmost layer spacings; the results are listed in Table II. The replacement of Mn by Al in the topmost plane leads to a slight improvement of the R factor from 0.43 to 0.37 (without applying the ATA). This R factor improvement may indicate some segregation of Al into the topmost layer, in accordance with the LEIS results described in the next section. Replacement of Mn by Al also in the second plane does not affect the R factor. We expect to get more details about chemical ordering by analyzing other surface orientations such as, for example, the twofold symmetric surface. In our preliminary investigations, the diffracted intensities of quasicrystalline twofold symmetric surfaces are in general very sensitive to the chemical identity of the atoms; it is even possible that intensities of some spots vanish completely without chemical ordering.

Finally, we describe results of calculations with a strongly corrugated surface with intact Mackay-type clusters. These calculations are motivated by the fact that there is evidence for surface roughness after cleaving *in situ*, with aggregates of Mackay-type clusters at the surface.[11] For the calculations, we used a termination of the group marked with arrows in Fig. 7, namely, the one with $z=-6.60$ Å. This termination contains many intact pseudo Mackay icosahedra in the sur-

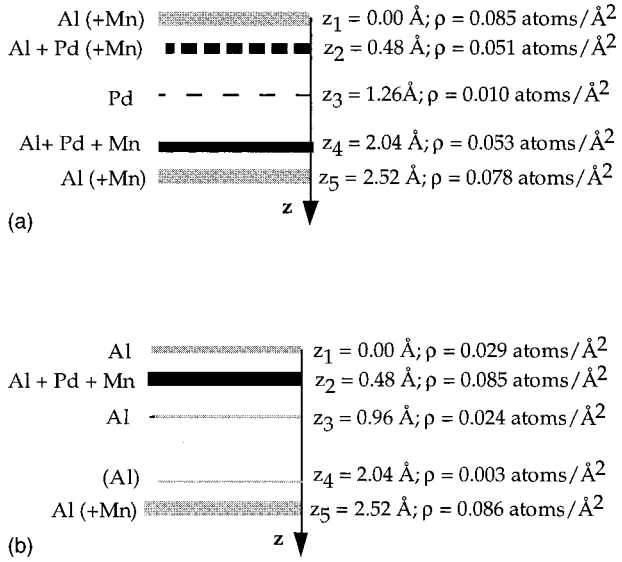

FIG. 8. Averaged lateral densities and bulk positions of the atomic planes (a) for the terminations marked by arrows in Fig. 6 (position of the topmost layer in Fig. 6: $z=-27.96$, -23.88; -17.28; -10.68; -6.60, 0.00; 4.08, 10.68, 17.28, and 27.96 Å), (b) for the terminations marked by squares in Fig. 6 (position of the topmost layer in Fig. 6: $z=-19.80$, -13.20, -2.52, 14.76, and 25.44 Å). The planes are drawn at their respective depths z, as bars with thickness proportional to the atomic density in each plane, together with their approximate composition as symbolized at bottom of figure (parentheses indicate minority species). The position of the topmost atomic plane is chosen as the origin for the z axis.

face region. In a first step, only atoms within the Mackay clusters were taken into account for the topmost planes. The topmost atoms of the clusters are located at $z=-6.60$ Å while the equatorial plane of the clusters consists of a ring with 10 atoms at $z=-2.04$ Å [Fig. 9(a)]. The equatorial plane is the first layer for which all atoms are taken into account in the calculation. An optimization of the topmost interlayer spacings led, however, to a bad R factor ($R=0.68$) so that this configuration can be ruled out.

In Fig. 9(a) one can see also fractions of ''10 rings'' in the equatorial plane that belong to fractions of Mackay-type clusters. By taking the atoms within these clusters additionally into account, one gets a surface with a higher density of the topmost planes, see Fig. 9(b). The R factor for this configuration is improved to 0.52.

The ''flat'' surface termination is shown in Fig. 9(c). A LEED calculation for this termination leads to an R value of 0.38, thus indicating that the surface is not strongly corrugated at an atomic level. One should note that one gets already 85% of the density of the topmost and second plane by taking the atoms of the Mackay-type clusters [Fig. 9(b)], the Pd atoms in the third plane [stars in Fig. 9(c)], and all atoms in the topmost layers which are coordinated to these Pd atoms.

In summary, our LEED structural analysis strongly suggests that the fivefold symmetric surface of icosahedral AlPdMn consists of densely packed, Al-rich terminations that are all very similar. The topmost atomic plane consists mainly of Al, mixed with about 10% Mn. One cannot rule out from the LEED analysis that the topmost layer consists only of Al. The second plane is a mixed Al-Pd layer with about 50% Al and 50% Pd. The topmost atomic plane is relaxed towards the bulk by 0.06 ± 0.04 Å, while the positions of the deeper layers are almost bulklike.

V. CORROBORATING EXPERIMENTAL DATA

In principle, LEIS is a quantitative technique that is uniquely sensitive to the elemental composition of the topmost surface layer. Therefore, we implemented LEIS as a check on the LEED structural results.

Experimental data from one LEIS experiment are shown in Fig. 10. For purposes of quantitative analysis, the instrument was calibrated to the pure elements using polycrystalline Mn, Al(111), and Pd(100). The three peaks in the spectrum of the quasicrystal at highest kinetic energy correspond to scattering from each of these three types of atoms, as labeled. At lowest kinetic energy, a small peak represents oxygen contamination. In principal, the intensities of individual peaks can be used to extract the atomic densities of individual species at the surface. This is done by comparing to intensities of pure elemental standards, which have known surface densities. The procedure assumes that relative sensitivity factors in ion scattering do not depend on chemical environment.[51]

TABLE III. Optimized Pendry R factor and z positions of the atomic planes after intensity mixing of terminations marked by squares in Fig. 6 and averaged chemical compositions (position of the topmost layer in Fig. 6: $z=-19.80$, -13.20, -2.52, 14.76, and 25.44 Å). Shown are the results for calculations with and without ATA.

		Optimum geometry	Chemical composition		
	R_P	Positions of topmost layers	layer 1	layer 2	layer 1+2
With ATA	0.45	$z_1=(-0.02\pm0.07)$ Å	100% Al	35% Al	52% Al
		$z_2=(0.47\pm0.07)$ Å	0% Pd	39% Pd	28% Pd
		$z_3=(0.96\pm0.15)$ Å	0% Mn	26% Mn	20% Mn
		$z_5=(2.50\pm0.10)$ Å			
Without ATA	0.57	$z_1=(0.08\pm0.07)$ Å			
		$z_2=(0.58\pm0.07)$ Å			
		$z_3=(1.00\pm0.15)$ Å			
		$z_5=(2.49\pm0.15)$ Å			

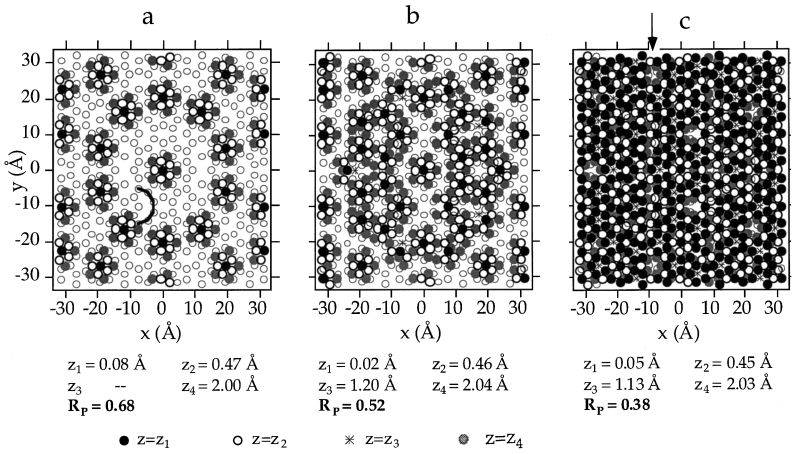

FIG. 9. Configurations used for the IV calculations for a rough surface, together with the *R* factor values and optimized layer positions (the origin corresponds to the position of the topmost layer in the unrelaxed configuration). For these configurations, the termination with $z=-6.60$ Å (see Fig. 6) was taken. (a) Only atoms within pseudo-Mackay icosahedra (PMI) were taken. Full circles: topmost atoms of the PMI; open circles: 2nd plane (0.48 Å underneath); grey circles: third plane (2.04 Å underneath). Grey, open circles: plane 4.56 Å underneath; this is the first plane where all atoms are taken into account in the IV calculation. The equatorial planes of the Mackay clusters lie within this plane and consist of rings with 10 atoms. Fractions of such rings, one of which is indicated by the solid line, belong to fractions of (overlapping) Mackay type clusters. Two further planes, located 2.52 and 4.08 Å underneath the topmost plane, are not shown. (b) Structure with higher density in the topmost layers, obtained by adding the atoms within the incomplete ''fractions'' of Mackay type clusters to Fig. 9(a). The stars are Pd atoms, lying 3.30 Å underneath the topmost plane. (c) complete, bulklike termination. Indicated by the arrow is a pentagonal hole. These holes are located at the nodes of a Fibonacci pentagrid, as well as the Mackay clusters of Fig. 9(a).

There are two main sources of uncertainty in extracting quantitative data from the LEIS data. First is the fact that the density of Mn atoms in the reference sample is unknown because of its polycrystallinity. An upper estimate of the surface density is probably 1.88×10^{15} atoms cm^{-2}, which is the $\frac{2}{3}$ root of the volume density; based on low-index surface densities of common single-crystal metals, we estimate that half this value is probably the lower limit. The second uncertainty comes from the fact that the background in the spectral region is rather large, as shown in Fig. 10. This background is attributed to multiple scattering in multicomponent systems. At one extreme, we have implemented a fifth-order polynomial fit of the background and subtracted this in calculating integrated peak intensities. (This is most similar to the background estimation suggested in the literature, which is simply a line drawn between valleys of adjoining peaks.[52,53]) The dashed line in Fig. 10 shows the polynomial approach. In the other approach no background was subtracted. The concentrations obtained with all these approaches are summarized in Table IV, which shows that uncertainties due to the Mn concentration and the background subtraction exceed the statistical uncertainties. The values in Table IV probably encompass the true concentrations. The result is that the Al concentration is 83.4–86.3%, Pd is 10.2–13.8%, and Mn is 0.4–6.3%. Hence, the surface layer is enriched in Al, and deficient in Pd, relative to the bulk concentrations. There is also depletion of Mn.

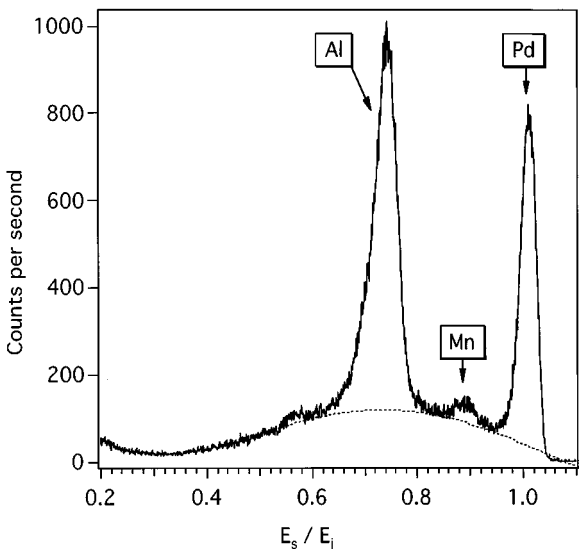

FIG. 10. Ion scattering spectra for a fivefold surface of icosahedral AlPdMn. The *x* axis shows the ratio of scattered ion energy E_s to incident ion energy E_i. The dashed line is a fifth-order polynomial, constrained to fit to the energy ratio ranges of about 0.20–0.52, 0.609–0.613, 0.82–0.83, and 1.04–1.10 eV.

If, as the LEED analysis suggests, the two top layers are separated by only 0.4 Å, LEIS may sample both layers. Its sensitivity to the second layer probably will be less than that of the top layer, but still significant. At this time, we cannot weight the contributions of these two layers quantitatively, but we can set limits. At one extreme, the second layer could be weighted equally with the top layer, yielding an average surface composition (from LEED) of $Al_{77}Pd_{15}Mn_8$; at the other extreme, the second layer could be invisible, yielding an average surface composition of $Al_{93}Pd_0Mn_7$. One would expect the real experimental result from LEIS to lie somewhere between these two extremes, which is true for the Al and Pd concentrations. (For Al, $77<83-86<93$, and for Pd, $0<10-14<15$). The Mn concentration, however, falls below the minimum value of 7% predicted from LEED, suggesting that there may be replacement of Mn by another metal—probably Al—at the surface sites.

TABLE IV. Surface concentrations of the metallic components, obtained from low-energy ion scattering spectroscopy. The table shows the way in which two different assumptions about the concentration of Mn in the standard, and two different approaches to background subtraction, affect the results. The uncertainties show plus/minus one standard deviation, derived from measurements on three separate samples.

Background Subtraction \ Concentration of Mn Standard	0.94×10^{15} atoms/cm^2	1.88×10^{15} atoms/cm^2
5th order polynomial	Al: 85.7±0.3%	Al: 85.1±0.2%
	Pd: 13.5±0.4%	Pd: 13.4±0.4%
	Mn: 0.7±0.3%	Mn: 1.4±0.5%
None	Al: 86.1±0.2%	Al: 83.8±0.4%
	Pd: 11.0±0.5%	Pd: 10.7±0.5%
	Mn: 2.8±0.4%	Mn: 5.5±0.8%

Therefore, we carried out LEED calculations also with Mn being replaced by Al in the topmost layer (see Sec. IV and Table II). These calculations showed that also a Mn depleted topmost layer is consistent with the results of the LEED analysis.

The LEIS result can also be used to rule out two classes of terminations in Fig. 7: the Pd-pure layers indicated by well-spaced dashes (since these would require the surface composition to be at least 50% in Pd); and many of the 50-50 AlPd layers represented by closely-spaced dashes (since many of these lie on top of a pure Pd layer, and hence would also require the composition to be no less than 50% Pd). A composition of 50% Pd in the surface layer falls well outside the furthest reasonable estimate of surface composition listed in Table IV.

In summary, an exact quantitative comparison between the LEIS data and the LEED model is not possible, partly because of uncertainties in extracting concentrations from the experimental data, and partly because of uncertainties about the degree to which each of the top two planes would contribute to the LEIS signal. Broadly, however, the LEIS results are consistent with the LEED structure analysis in that LEIS indicates an aluminum-rich composition. Also in agreement with LEED, the LEIS results serve to exclude certain Pd-rich classes of terminations.

VI. DISCUSSION

Some of the properties of the quasicrystalline surface geometry found in this analysis can be understood in terms of principles known to govern the structures of periodic crystalline metals. In general, for example, close packed metal surfaces are most stable, and this appears to hold also for the icosahedral AlPdMn quasicrystal. STM and LEED measurements of Schaub *et al.*, who investigated the surface structure of microfacets that formed on the twofold surface of the AlPdMn icosahedral alloy upon heating in vacuum,[4,5] revealed that microfacets grown perpendicular to a fivefold axis prevail. As shown in our LEED analysis, the fivefold symmetrical surface consists of rather densely packed terminations: the two-dimensional density of the topmost two atomic planes combined together is about 0.136 atoms/Å^2, compared to the value of 0.141 atoms/Å^2 for one plane of the close packed Al(111) surface.

The Al-rich terminations found here also correlate with factors known to govern surface compositions of crystalline alloys. At those simpler surfaces, one finds preferential segregation by components with the lower surface free energy, larger atomic volume, and more positive heat of solution.[54] (Surface free energy typically is the dominant factor.) The Al-rich terminations found here are expected if these factors are taken into account.[54,55]

Our LEED structural analysis, as well as the STM measurements by Schaub *et al.*, point towards an atomically flat surface after the surface treatment with sputtering and annealing as described above.[4–6] While the LEED IV data are consistent with a surface that is flat on an atomic level, the sharpness of the LEED spots indicates that the ordered part of the surface is not rough on a larger scale of several 100 Å (the coherence length of the LEED beam). Otherwise, one would expect a broadening of the spots due to the worsening of the lateral long-range order. In contrast, STM investigations of Al-Pd-Mn prepared by *in situ* cleavage revealed significant atomic scale roughness.[11] In that study, the surface structure was found to be determined by cluster aggregates formed on the basis of an elementary cluster whose diameter of about 10 Å points to the pseudo-Mackay icosahedron (PMI). Although the surface morphology is different, there is evidence that many of the Mackay-type clusters are present also in the structure we found by LEED; they are, however, embedded within an Al-rich surface layer. This can be seen for example with the termination shown in Fig. 9. It is also instructive to compare the positions of the topmost atomic planes with the vertical positions of atoms in a PMI oriented along a fivefold axis. It turns out that each plane of the Mackay cluster has its counterpart in the AlPdMn surface structure (see Fig. 11). This gives evidence for many intact pseudo-Mackay clusters in the surface region, with some of the atoms in the surface layer being the topmost atom of a PMI and the others filling in the spaces between the PMIs to yield a flat surface. These findings are in line with recent photoelectron diffraction experiments that gave direct evidence for the existence of pseudo-Mackay icosahedra in the surface region.[19]

The terminations found in this structure analysis compare well with the step structure seen with STM. We found a mix of very similar terminations, many of which are separated by steps with heights of 4.08 Å or 6.60 Å, as observed also with STM. Next, we try to correlate other surface features seen with STM to local structures in our model. In the STM study,[4,5] fivefold symmetric holes with quasiperiodic long-range order were found; they have the same orientation on

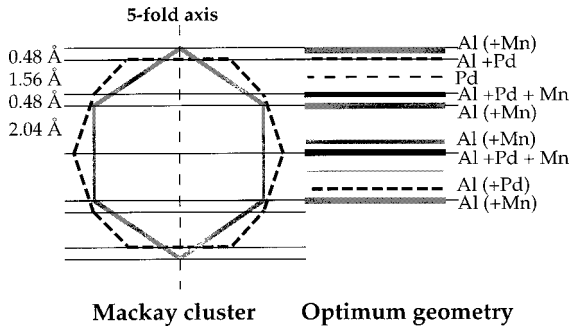

FIG. 11. The geometry of a pseudo-Mackay icosahedron (PMI) oriented along a fivefold symmatric axis, compared with the layer sequence of the optimum terminations determined in the LEED analysis. Grey: dodecahedron, black: icosidodecahedron of the Mackay cluster (the small dodecahedron, with atoms lying 2.52 Å underneath the topmost atom, is not shown). Each plane of the Mackay cluster has its counterpart in the Al-Pd-Mn surface structure. The topmost layer of the structure found by LEED coincides with the topmost plane of many Mackay icosahedra.

all terraces. By connecting their edges with straight lines, a Fibonacci pentagrid with line separations of 7.38 Å and 11.94 Å can be constructed. Fivefold symmetric clusters with a similar quasiperiodic long-range order can be discerned also in the surface terminations that we found by LEED. The Mackay-type clusters of Fig. 9(a), for example, lie on such a Fibonacci pentagrid. With the densely packed surface of Fig. 9(c), only their topmost two planes are exposed to the surface, showing up as pentagons with an Al atom in the topmost plane, surrounded by five Al or Pd atoms about 0.4 Å underneath. These Al/Pd pentagons can be seen for all terminations we found, and their orientation is always the same. Another fivefold symmetric feature is the deeper and larger fivefold symmetric hole marked by the arrow in Fig. 9(c). These holes are also located on the nodes of a Fibonacci pentagrid and have the same orientation for all terminations (however, they have very low density for some terminations). One may speculate that one of those two features gives rise to the appearance of the fivefold symmetric holes in STM.

In summary, we have described a first attempt at solving the surface structure of a radically new class of materials, by adapting and utilizing techniques that are known to work for more traditional materials. According to the traditional benchmark of such analyses, the *R* factor, a successful result has been obtained. However, there is undoubtedly much more to be learned. In order to refine and test this approach, it will be necessary to apply it to other types of quasicrystalline surfaces, and to always compare the results with data from complementary experimental techniques. We are now beginning such analyses for the twofold surface of icosahedral AlPdMn, and for the fivefold surface of icosahedral AlCuFe.

ACKNOWLEDGMENTS

We thank M. de Boissieu for supplying information about the atomic planes in AlPdMn as well as the software used to generate the three-dimensional atomic bulk positions. This work was supported in large part by the Director, Office of Energy Research, Office of Basic Energy Sciences, Materials Sciences Division, of the U.S. Department of Energy under Contracts Nos. DE-AC03-76SF00098 and W-405-Eng-82. M.G. acknowledges financial support from the German DFG.

*Present address: Institut für Kristallographie und Mineralogie der Universität München, Theresienstr. 41, D-80333 München, Germany.

[1] E. G. McRae, R. A. Malic, T. H. Lalonde, F. A. Thiel, H. S. Chen, and A. R. Kortan, Phys. Rev. Lett. **65**, 883 (1990).

[2] A. R. Kortan, R. S. Becker, F. A. Thiel, and H. S. Chen, Phys. Rev. Lett. **64**, 200 (1990).

[3] R. S. Becker and A. R. Kortan, in *Quasicrystals: The State of the Art*, edited by D. P. DiVincenzo and P. Steinhardt (World Scientific, Singapore, 1991), p. 111.

[4] T. M. Schaub, D. E. Bürgler, H.-J. Güntherodt, and J. B. Suck, Phys. Rev. Lett. **73**, 1255 (1994).

[5] T. M. Schaub, D. E. Bürgler, H.-J. Güntherodt, and J.-B. Suck, Z. Phys. B **96**, 93 (1994).

[6] T. M. Schaub, D. E. Bürgler, H.-J. Güntherodt, J. B. Suck, and M. Audier, Appl. Phys. A: Solids Surf. **61**, 491 (1995).

[7] T. M. Schaub, D. E. Bürgler, H.-J. Güntherodt, J. B. Suck, and M. Audier, in *Proceedings of the 5th International Conference on Quasicrystals*, edited by C. Janot and R. Mosseri (World Scientific, Singapore, 1995), p. 132–138.

[8] S.-L. Chang, W. B. Chin, C.-M. Zhang, C. J. Jenks, and P. A. Thiel, Surf. Sci. **337**, 135 (1995).

[9] S.-L. Chang, J. W. Anderegg, and P. A. Thiel, J. Non-Cryst. Solids **195**, 95 (1996).

[10] C. J. Jenks, S.-L. Chang, J. W. Anderegg, P. A. Thiel, and D. W. Lynch, Phys. Rev. B **54**, 6301 (1996).

[11] P. Ebert, M. Feuerbacher, N. Tamura, M. Wollgarten, and K. Urban, Phys. Rev. Lett. **77**, 3827 (1996).

[12] M. Gierer, M. A. Van Hove, A. I. Goldman, Z. Shen, S.-L. Chang, C. J. Jenks, C.-M. Zhang, and P. A. Thiel, Phys. Rev. Lett. **78**, 467 (1997).

[13] Z. Shen, C. J. Jenks, J. Anderegg, D. W. Delaney, T. A. Lograsso, P. A. Thiel, and A. I. Goldman, Phys. Rev. Lett. **78**, 1050 (1997).

[14] M. Erbudak, H.-U. Nissen, E. Wetli, M. Hochstrasser, and S. Ritsch, Phys. Rev. Lett. **72**, 3037 (1994).

[15] S. Suzuki, Y. Waseda, N. Tamura, and K. Urban, Scr. Metall. Mater. **35**, 891 (1996).

[16] M. Zurkirch, A. Atrei, M. Hochstrasser, M. Erbudak, and A. R. Kortan, J. Electron Spectrosc. Relat. Phenom. **77**, 233 (1996).

[17] Z. Shen, P. J. Pinhero, T. A. Lograsso, D. W. Delaney, C. J. Jenks, and P. A. Thiel, Surf. Sci. Lett. **385**, L923 (1997).

[18] J. Chevrier, G. Cappello, F. Comin, and J. P. Palmari, in *Proceedings of the Conference on New Horizons in Quasicrystals: Research and Applications*, edited by A. I. Goldman, D. J. Sordelet, P. A. Thiel, and J. M. Dubois (World Scientific, Singapore, 1997), pp. 144–151.

[19] D. Naumovic, P. Aebi, L. Schlapbach and C. Beeli, in *Proceedings of the Conference on New Horizons in Quasicrystals: Research and Applications* (Ref. 18), pp. 86–94.

[20] D. Naumovic, P. Aebi, L. Schlapbach, C. Beeli, T. A. Lograso, and D. W. Delaney, in *Proceedings of the Sixth International*

Conference on Quasicrystals (ICQ6), edited by T. Fujiwara and S. Takeuchi (World Scientific, Singapore, 1998).
[21] F. Shi, Z. Shen, D. W. Delaney, A. I. Goldman, C. J. Jenks, M. J. Kramer, T. Lograsso, P. A. Thiel, and M. A. Van Hove (unpublished).
[22] Y. Yokoyama, A.-P. Tsai, A. Inoue, and T. Masumoto, Mater. Trans., JIM **32**, 1089 (1991).
[23] Y. Yokoyama, T. Miura, A.-P. Tsai, A. Inoue, and T. Masumoto, Mater. Trans., JIM **33**, 97 (1992).
[24] M. de Boissieu, M. Durand-Charré, P. Bastie, A. Carabelli, M. Boudard, M. Bessière, S. Lefèbvre, C. Janot, and M. Audier, Philos. Mag. Lett. **65**, 147 (1992).
[25] C. Beeli and H.-U. Nissen, Philos. Mag. B **68**, 487 (1993).
[26] M. Audier, M. Durand-Charré, and M. de Boissieu, Philos. Mag. B **68**, 607 (1993).
[27] M. Boudard, E. Bourgeat-Lami, M. de Boissieu, C. Janot, M. Durand-Charré, H. Klein, M. Audier, and B. Hennion, Philos. Mag. Lett. **71**, 11 (1995).
[28] T. A. Lograsso and D. W. Delaney, J. Mater. Res. **11**, 2125 (1996).
[29] S.-S. Kang and J.-M. Dubois, J. Mater. Res. **10**, 1071 (1995).
[30] J.-M. Dubois, S. S. Kang, and Y. Massiani, J. Non-Cryst. Solids **153-4**, 443 (1993).
[31] S. S. Kang, J. M. Dubois, and J. von Stebut, J. Mater. Res. **8**, 2471 (1993).
[32] J.-M. Dubois, S. S. Kang, and A. Perrot, Mater. Sci. Eng. A **179/180**, 122 (1994).
[33] A. I. Goldman and M. Widom, Annu. Rev. Phys. Chem. **42**, 685 (1991).
[34] A. I. Goldman and K. F. Kelton, Rev. Mod. Phys. **65**, 213 (1993).
[35] C. Janot, in *Quasicrystals: A Primer*, edited by C. J. Humphreys, P. B. Hirsch, N. F. Mott, and R. J. Brook (Clarendon, Oxford, 1992).
[36] P. R. Watson, M. A. Van Hove, and K. Hermann, *NIST Surface Structure Database Ver. 2.0* (NIST Standard Reference Data Program, Gaithersburg, Maryland, 1996).
[37] Y. Gauthier, Surf. Rev. Lett. **3**, 1663 (1996).
[38] C. J. Jenks, D. Delaney, T. Bloomer, S.-L. Chang, T. Lograsso, and P. A. Thiel, Appl. Surf. Sci. **103**, 485 (1996).
[39] O. L. Warren and P. A. Thiel, Phys. Rev. B **47**, 10 848 (1993).
[40] M. Boudard, M. de Boissieu, C. Janot, G. Heger, C. Beeli, H. U. Nissen, H. Vincent, R. Ibberson, M. Audier, and J. M. Dubois, J. Phys. C **4**, 10 149 (1992).
[41] M. de Boissieu (private communication).
[42] F. Jona, K. O. Legg, H. D. Shih, D. W. Jepsen, and P. M. Marcus, Phys. Rev. Lett. **40**, 1466 (1978).
[43] P. J. Rous, Surf. Sci. **244**, L137 (1991).
[44] M. A. Van Hove, W. H. Weinberg, and C.-M. Chan, in *Low-Energy Electron Diffraction: Experiment, Theory and Surface Structure Determination, Vol. 6 of Springer Series in Surface Sciences*, edited by G. Ertl and R. Gomer (Springer-Verlag, Berlin, 1986).
[45] H. D. Shih and S. W. Tam, in *Determination of Surface Structures by LEED*, edited by P. M. Marcus and F. Jona (Plenum, New York, 1980).
[46] D. Aberdam, R. Baudoing, and C. Gaubert, Surf. Sci. **52**, 125 (1975).
[47] K. Heinz and G. Besold, Surf. Sci. **125**, 515 (1983).
[48] W. Moritz, J. Phys. C **13**, 353 (1984).
[49] J. Pendry, J. Phys. C **13**, 937 (1980).
[50] A. Wander, J. B. Pendry, and M. A. Van Hove, Phys. Rev. B **46**, 9897 (1992).
[51] R. Souda, T. Aizawa, C. Oshima, S. Otani, and Y. Ishizawa, Phys. Rev. B **40**, 4119 (1989).
[52] C. Creemers, D. Royer, and P. Schryvers, Surf. Interface Anal. **20**, 233 (1993).
[53] J. C. Bertoloni, J. L. Rousset, P. Miegge, J. Massardier, B. Tardy, Y. Samson, B. C. Khanra, and C. Creemers, Surf. Sci. **281**, 102 (1993).
[54] A. R. Miedema, Z. Metallkd. **69**, 287 (1978).
[55] A. R. Miedema, F. R. deBoer, and R. Boom, CALPHAD: Comput. Coupling Phase Diagrams Thermochem. **1**, 341 (1977).